Chapter 12: The energy signature cratering model

Abstract

The concept of an energy signature specific to shock-release wave pairs is proposed as an additional evidence to identify impact craters. The movement from extreme high to extreme low by way of an adiabatic dispersion leaves a distinct pattern which I will label a “release wave valley” in topography and gravity readings. Examples of this unique expression are discussed on the Moon, Venus and Earth and their association with impact cratering is pointed out. The cratering process is analyzed to determine where this adiabatic response occurs, and to develop a cratering mechanism around it.

Introduction

Looking at the vast majority of all moon craters on the GRAIL map, the map that shows the density of the rock, they have blue bottoms (low density) and red or yellow rims (high density) [Chapter 10A]. While the rims show the effect of high compressional energy, the crater’s bottoms show the opposite effect of expansion energy. If a crater was formed by just a compressional wave that was pushing the rock out and blasted ballistic ejecta even further as Shoemaker (1974) proposed with the cratering model still used by NASA (see Chapter 8, Figure 8.3), would it not have compressed the bottom of the crater the same way it did the rim and produce a high gravity reading across the entire crater?

The form of a shock-release wave

From the Greek word *kryptos*: where something is hidden or put out of sight, the word “cryptoexplosions” was coined for the force forming craters that were later recognized as meteor impact structures (French 1998). It is now recognize that these craters are not the result of an explosion but a shock wave. While the image of a shockwave generated by an explosion, as in Figure 12.1, still lingers in our memory, the method of production larger craters is very different. A meteor is traveling at 10-20 km per second, about 3,600 -7,200 km/hour (2,237 – 4,474 mph), almost 3-6 times the speed of sound (Mach 3-6). Upon striking the surface of the planet produces much more than just an explosion. The energy of the rapidly moving object is turned into work. This work is accomplished as the extremely brief elevated compressional energy of a shock wave descends immediately into slightly more elongated extremely depressed expansional energy of a release wave, a type of rarefaction wave (Figure 1.3). This movement from shock wave to release wave and the adiabatic work it accomplishes is what sets impact craters apart.

The shock wave can actually be seen as it compresses the air around the explosion of a small bomb (Figure 12.1) and as long as the expression of the shockwave does not greatly exceed the size of the explosion, we can think of it as only explosive energy.

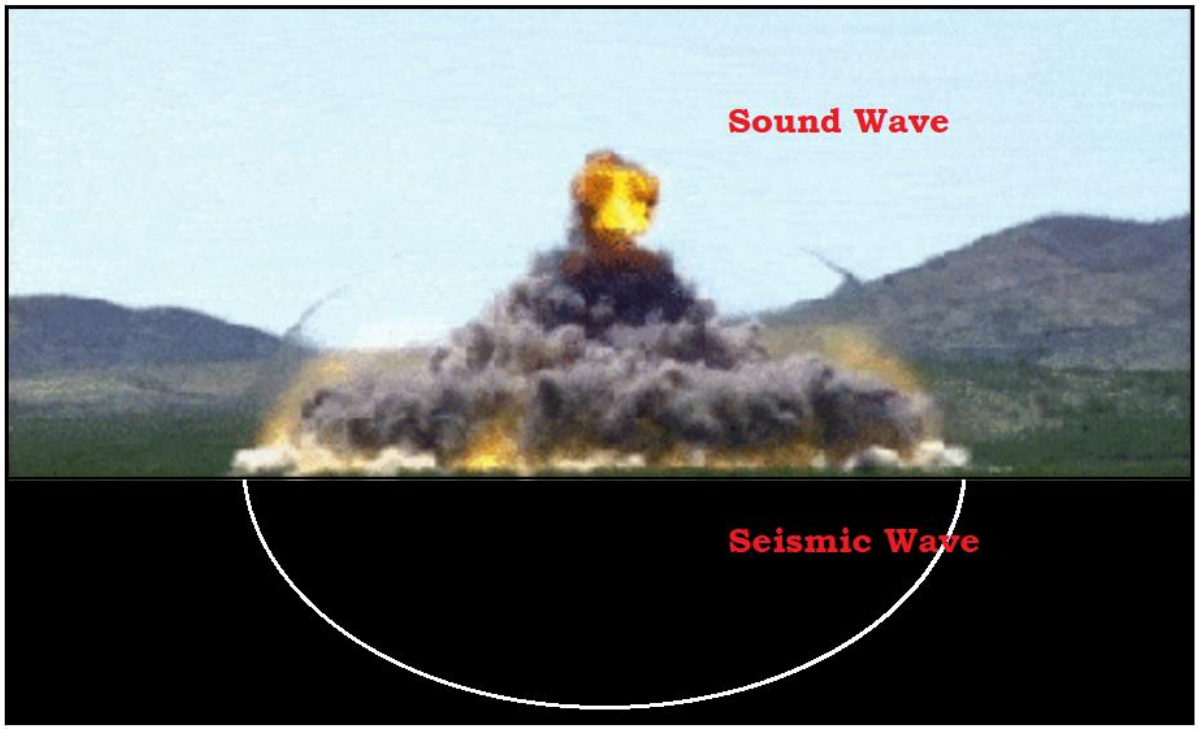

Figure 12.1: Shock wave produced by the explosion of a small bomb. Upper portion of wave made visible where it distorts the view just above the mountains against the sky. It travels as both a sound wave in air and a seismic wave through the ground.

Shock waves are well represented in modern times by the explosive eruption of Krakatoa Volcano. When it erupted in 1883 it produced a shockwave that circled the globe repeatedly for 5.6 days before the waves shape was lost in the background energy noise (Strachey. 1888). The passing waves were graphed at numerous seismic stations worldwide, Figure 3.6. The wave’s shape shows *the energy’s rapid rise and immediate plunge,* mapped in all shock wave as represented in Figure 1.3, *with its accompanying adiabatic dispersion* in larger shock-release waves leaves a related visible form in the resulting crater. I will refer to this shape as the *energy signature* of a shockwave.

A complete energy signature contains three elements: 1) the energy’s rapid rise 2) immediate plunge 3) evidence by adiabatic work resulting in dispersion of breccia/ejecta within the area of the energy plunge.

The energy signature of a shock-release wave pair without the adiabatic dispersal is illustrated by a skipping rock on a lake. Figure 12.2 shows a disc substituted for the rock in a standardized experimental setting. The disc arrives at an oblique angle, represented by the red line and arrow, and excavated a linear groove in the water's surface. The shock wave, represented by the hollow sphere of water indicated by the yellow arrow, was produced behind the disc. As that shock bubble is centered at the point where the disc contacted the water, that was where a portion of the forward energy was converted to a shock wave, and the disc was actually allowed to escape. Once the shockwave was produced, its energy moved outwards beyond the linear groove produced by the impact and forms the ripples with its energy. Here, the ripple is the energy signature of a shock and release wave.

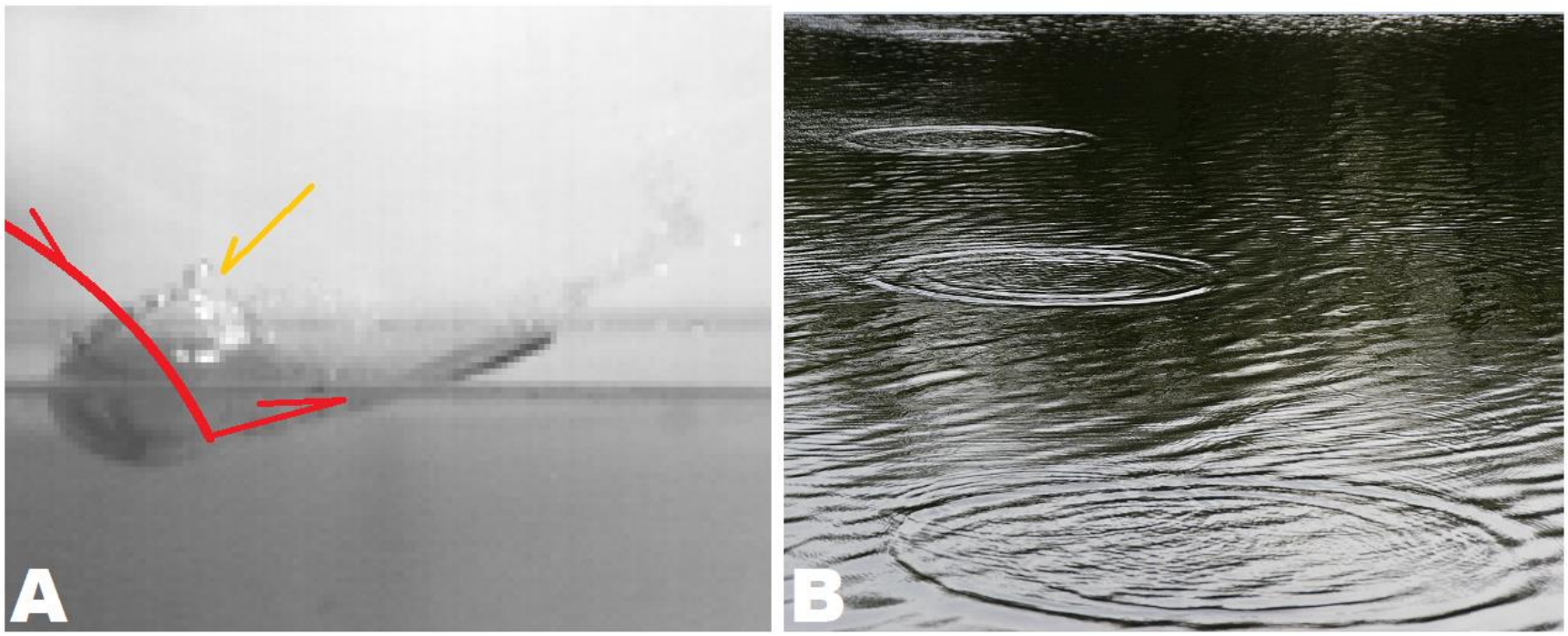

Figure 12.2: Skipping stone showing shock wave in (A) and circular ring of energy signature from the shock-release wave know as ripples (Image 6, Figure 1, Clanet et al 2004).

Seeing the shock-release wave

The shock-release wave generated in an impact rises so rapidly to its peak stress energy and plunges immediately to such lows that it leaves a permanent mark on the substrate which is not consistent with the slow geological processes near ambient temperatures which are generally postulated as taking place on earth today. Indeed, if a comparable number of impact craters seen on the moon took place on the earth the entire surface of our planet has been shaped by their energy expression. It is possible that slow, near ambient geological process over large area have never taken place at all.

There are six criteria for impact crater recognition presently accepted by the Earth Impact Database, the generally recognized arbitrators of astral-crater recognition. The presence of 1) Shatter Cones, 2) Planar Deformation Features (PDFs), 3) High pressure mineral polymorphs, 4) Circular shape, 5) Impact melt, sheets, dikes, and breccias, and 6) Pseudotachylytes. They identify shatter cones and PDFs as being the most definitive because both of them are believed to be exclusively produced by shock waves. Since recognizing impact craters center around recognizing these shock-release wave structures on craters <200 km, it is important to ask, what would be the shock-release wave clues in a 2000 km crater or even a mere 800 - 1500 km diameter? Are these 6 characteristic adequate?

Circular Shape

Since even skipping rocks shows shock waves are circular (Figure 12.2), this is the most basic assumption for a shock formed structure. In his observation, Galileo recognized this circularity and named the moon's depression after the large Greek wine cup, a "krater". Volcanic craters are also said to have a circular shape, but are seldom perfectly circular. Two significant exception are Yellowstone crater/caldera, Figure 9.14, and Mount Tehama, the ancient mega volcano that preceded Mount Lassen volcano in the Sierra Nevada Mountains of California (see Chapter 7). The explosion that blew the head off Tehama left a perfectly circular caldera of about 6 km diameter with multiple circular annulus up to 35 km away, Figure 12.3. The Tehama annulus have clear highs under the white rings followed, towards the original shear point, consistently by dark lows in the northwestern, northeastern, and southeastern quadrants. It gives a circular shape but produces no adiabatic dispersion of breccia, except the volcanic breccia, which may offer a different explanation for the source of lava in larger volcanoes. The lithology acted like water in comparison to the energy released, leaving a ripples pattern in gravity maps, Chapters 9-10.

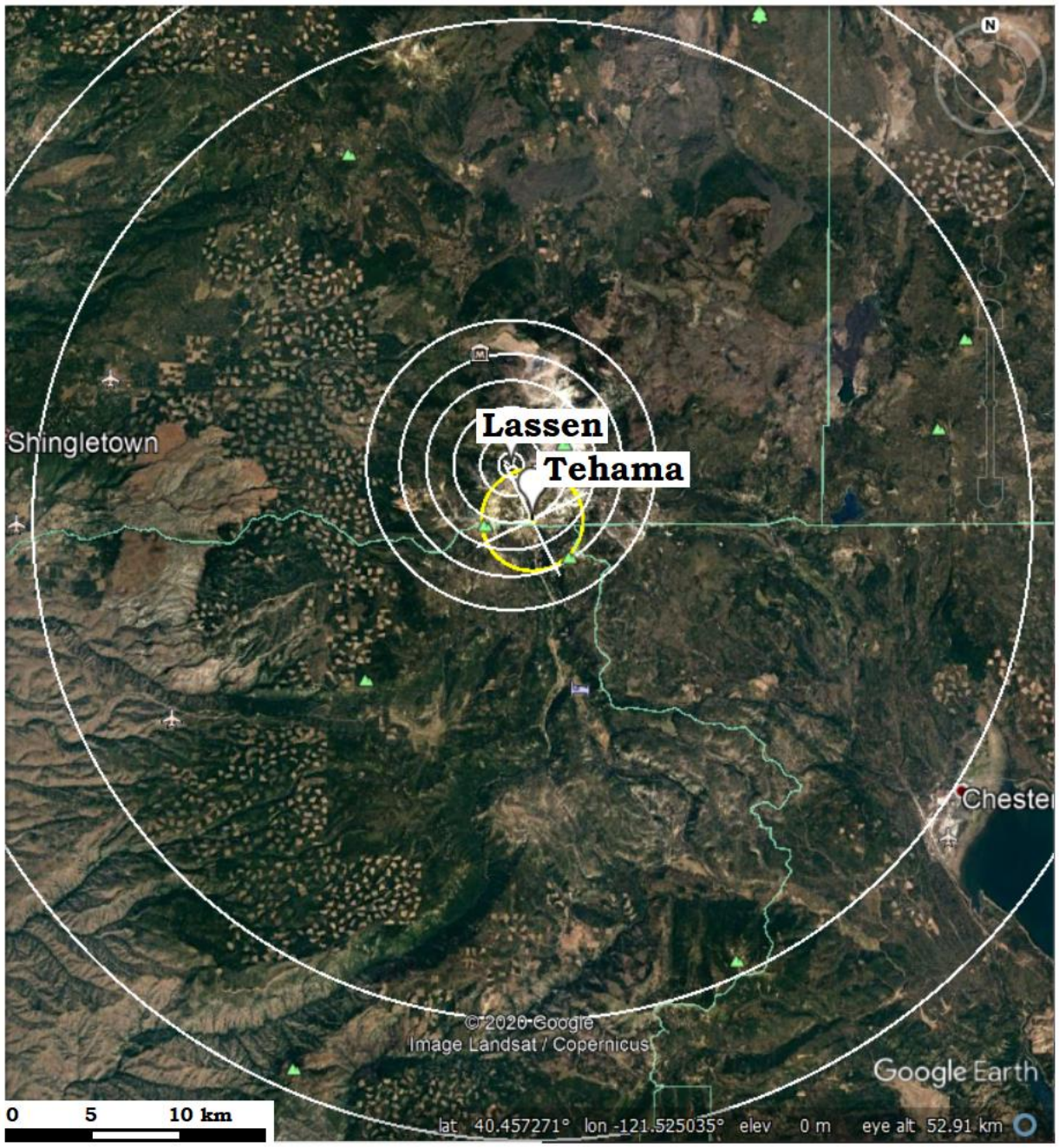

Figure 12.3: Shock pressure ridges mapped in the vicinity of Mount Lassen. Mount Tehama caldera, yellow circle, and its much larger shock pressure ridges of distant annulus, especially visible to the northeast, southeast and northwest quadrants.

High pressure mineral polymorphs

Coesite, stishovite, and diamonds and other high pressure minerals may have formed at great depth and been delivered to the surface by tectonics and other slow geologic processes (French 1998). But, these same high temperature, high pressure polymorphs could have formed in the myriad of shock-release wave energy envelopes of unrecognized impacts that Chapter 11 suggest, especially if tectonic forces are not operating. The diamonds found among the gold beneath the Vredefort Dome ghost crater, South Africa is such an occurrence. And, while the diamonds are connected with a crater, it is a much larger crater Koster crater that produced the entire Kaapvaal Basin than the Vredefort Dome crater.

Kink bands in Mica, a high pressure polymorph form, are common in impact craters, but also recognized in “normal” tectonic situations (French 1998). These “tectonic situations” may be unrecognized large impact craters. It all depends on the whether we are recognizing the pressure rings of the shock-release wave.

Planar Deformation Features

PDFs form only in quartz or feldspar minerals and can be recognized extending over distances of meters or tens of meters, although they become more erratic over distances of more than a centimeter. Showing an undulating pattern, and several apparent directions of cleavage in multi-centimeter samples of Coconino Sandstone adjoining the Meteor Crater in Arizona (French 1998).

While the structural identification of PDFs is very specific, requiring high magnification microscopes, they are thought to be definite proof of impact pressures (Figure 12.5). Yet, there are some problem with their occurrence. They have been twice found near the site of the supposed midair explosion of a bolide in 1908 over Tunguska, Siberia (Vannuchi et al 2015 and Hryanina, L.P., 1999.). No crater forming on impact was recognized by either author. Also, PDFs were found in lightning fulgurite (Giere et al 2015), suggesting other shock wave sources for their origin. If PDFs can originate from other than impact cratering sources, they are not as definitive as the Earth Impact Data Base assumes.

Two to five multiple sets of overlapping PDFs are found in a single sample, suggesting mobile grains or multiple close centers of shock energy are affecting each grain. As most PDFs do not span the entire grain, extinction of individual PDF linears is always observed (Figure 12.4). If extinction of PDFs relates to successive sets of fracturing then the heat of the second source over prints and anneals

the PDFs in their vicinity, but they happen together in such a short time that the heat of the first also overprints and anneals some of the second set of PDFs. This means a particular sample does not record the occurrence of only one crater but multiples in close proximity, up to the number of sets of PDFs seen.

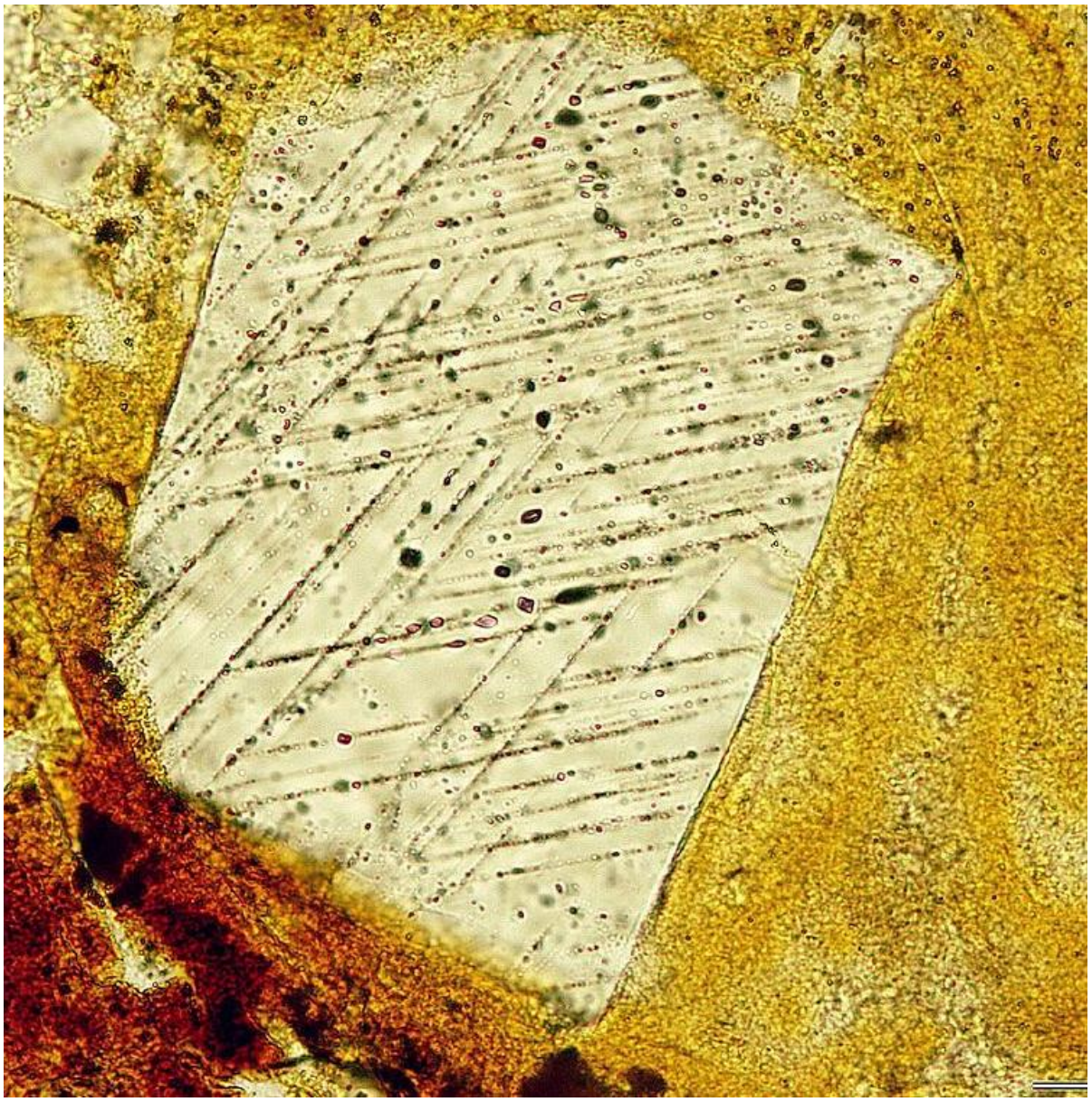

Figure 12.4: Two overlapping sets of PDF's in a matrix of cryptocrystalline quartz in impact melt from Suvasvesi South Impact structure, Finland. (Image credit: CC. by M. Schmeider, Wikipedia.)

The occurrence of Hematite could be the source of the red to brown coloring in the cryptocrystalline quartz matrix and spotting throughout the fractured quartz crystal. "Toasting" with hematite (Figure 12.5) is a common occurrence around PDFs as O_2 and Fe^{+3} unite with in the macro range. It requires only the presence of iron and high heat, 850+^{o}C, to produce the Fe+3 so that it will combine with any free oxygen, which may be freed from the silica dioxide (quartz) or free oxygen coming in through pressure opening of the PDFs.

Figure 12.5: Two samples of toasted quartz from Minthorn Impact structure Lake Elsinore, California, U.S.A. with quarter for size comparison.

PDFs often degenerate into planar fractures (PF) which can degenerate into cleavages and open cracks. As PF, cleavages and open cracks are also attributed to tectonic forces, they are not considered diagnostic of shock waves. However, cleavages that can be traced back to a shear center need to be considered as impact related, especially if there are multiple sets of PFs, because, tectonic forces would not be expected to act radially in opposing directions.

Shatter Cones

Shatter cones are identified by “horsetailing” or striated “cone-in-cone” structure, Figure 12.7. They are found below the base of the crater and often in any central uplift. On larger craters, shatter cones are located on rings of the crater (Watchorn 2013).

When cratering reaches down to the Moho (Lunar Discontinuity on the moon) and then into the upper mantle, how do you look for shatter cones or PDFs below that depth? Such craters are likely to produce some movement or give the appearance of movement, so that they would be mistaken for tectonic or continental motion. We can see movement of the shock wave rim by subsequent cratering at the Altai Scarp, the OCR of Mare Nectaris (Figure 8.8-10). Then the OCR evidences of cratering will be mistaken for evidences of tectonic motion.

In Figure 12.6 is the ION seismic section across the Sigsbee Scarp, Gulf of Mexico. The stratified layers at the top on both edges not only drop in the center, the scarp, but give way to considerable confusion. The lower two-thirds of the section shows distinct cone-in-cone structure. Is this what a shatter cone would look like in situ if it were sliced across? Is this a shatter cone for a crater as large as the Gulf of Mexico situated on a ring of the MCR crater, Figures 10.31 and 32?

Reis Crater, Germany

Steinheim Basin, Germany

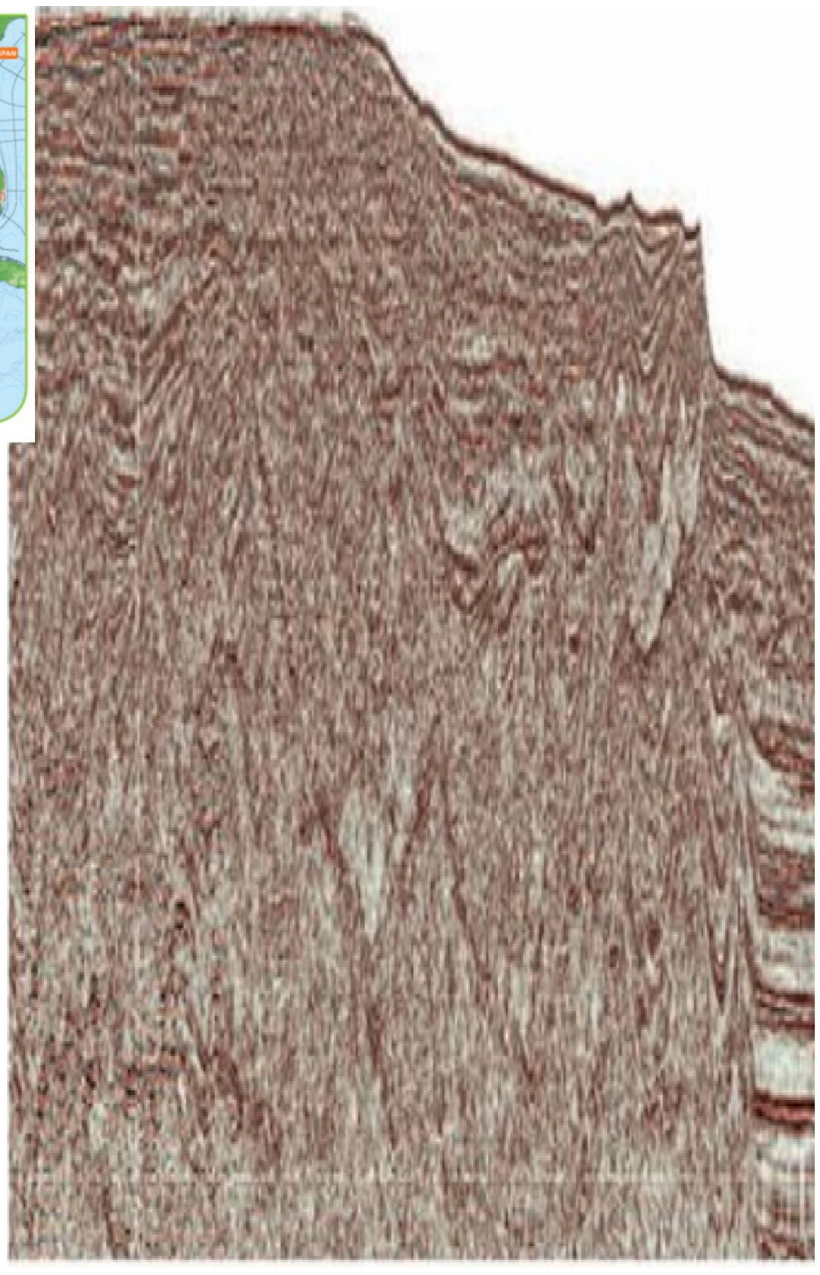

Figure 12.6: Seismic section (~200 km width x 12-14 km depth) across the Sigsbee Scarp showing stratified layers on the north and south edges, changing to cone-in-cone form in center. Examples of Shatter Cones from two cratering basins showing cone-in-cone or ‘horsetail” structure. (Image credit: Shatter cones by J. Baier, CC, Wikipedia. Seismic section Gulf of Mexico, ION.)

Iron oxides coloring

To understand the significance of color changes in Figures 12.4, 5, and 7, it is important to understand how iron oxides react when exposed to heat within a lithic body. There are three oxides of iron: magnetite (Fe_3O_4), hematite (Fe_2O_3), and rust ($4Fe + 3O_2 + 6H_2O$ –› $4Fe(OH)_3$). When iron sparks at room temperatures, a speck of magnetite is produced. Magnetite is a mineral that uses one unit of reduced iron (Fe^{+2}) and two units of oxidizes iron (Fe^{+3}) in its crystalline lattice. Hematite is a mineral that uses only oxidized iron (Fe^{+3}) in its lattice. Obviously, hematite requires a greater abundance of oxygen but it also requires being brought to a higher temperature to release the additional electron and allow all Fe ions to reach the +3 oxidation state. Because of the temperature at which it forms, hematite will disperse in quartz to color it (Figure 12.9). Magnetite may form near the temperature at which quartz

crystallized, but it will form separate crystals and deposit into a mixed crystal matrix (Africano et al 2002), like the quartzite in Figure 12.9.

Rust is a different kind of crystal as it contains water (hydroxide ions) in its crystal lattice. It forms when iron is exposed to water and cannot form at high temperature because the water is driven off. When rust is exposed to high temperature, it will degrade to atomic iron. Rust does not naturally adhere to quartz surface but requires a calcite carrier to attach it.

In ceramics a "Δ" stands for "cone," the temperature to which a clay body and its glaze are raised. Using Δ 6, ~1220ºC (2228ºF), magnetite crystals put into clay disappeared when fired, and when put into glaze remained dark spots. Within the clay body, the magnetite turned clear as it cooled without oxygen to atomic iron. Within the glaze, it reunited with oxygen to reform more dispersed magnetite spots when dissolved in the glass glaze. Using Δ10, ~1300ºC, (2372ºF), when magnetite crystals were put into clay it disappeared within the body of the clay and turned the entire surface, and only the surface, of the clay dark red to brown when fired. When it is put into glaze it formed brown or red spots. Within the body of the clay with a complete absence of oxygen it formed iron atoms, but where it could get to oxygen, it was forming hematite, the depth of color dependent on the quantity of oxygen it could obtain (Figure 12 .7). These results were true for mineral magnetite, andesite (Figure 12.8), and olivine rock (another mineral that contains reduced iron).

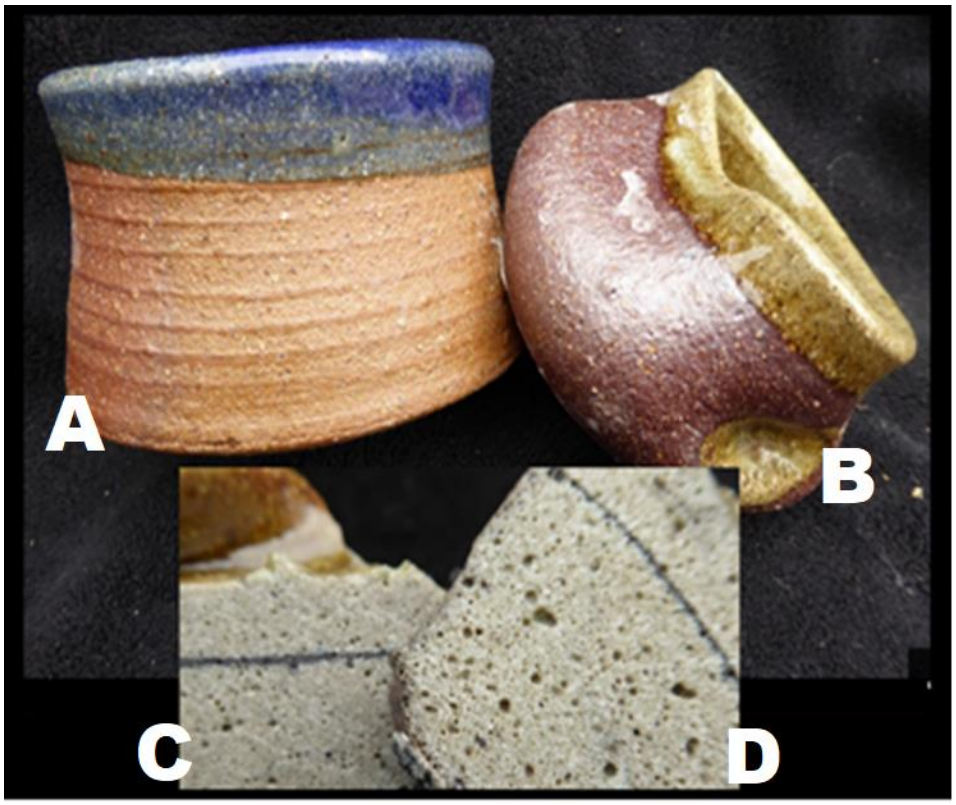

Figure 12.7: Upper, beakers and lower, sliced samples of clay body. All prepared from a clay body extremely high in magnetite. A & C fired to Δ10 with poor oxygen. B & D fired to Δ8, ~1271ºC/2320ºF with abundant oxygen. Dark line across C & D is trapped layer of glaze, high quartz and feldspar, between collapsed layers of clay. Trapped glaze layer shows no development of hematite. Large dark spots in clay body are voids.

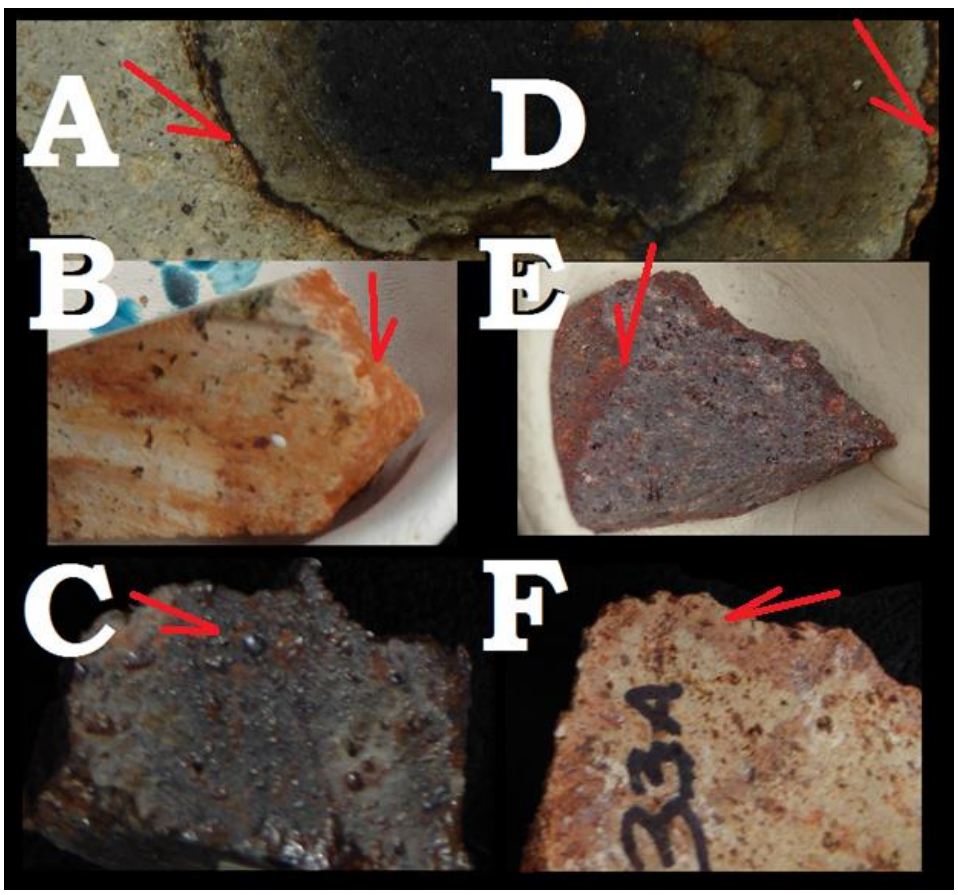

Figure 12.8: Andesite sample, "A" region is iron-feldspar rich, "D" region is iron-hornblende rich. "B & C" are feldspar rich and "E & F" were hornblende rich. Red arrows indicate hematite layer between regions in original sample. Hornblende contains water and loses it at high temperature. B) Raised to 1010ºC/1850ºF with little color change from iron. F) Raised to 1060ºC/1940ºF with abundant oxygen. E) Raised to 1222ºC and magnetite replaces hornblende as dark mineral. C) Raised to 1305ºC/2381ºF reduction with very limited oxygen, sheen is believed to be reflected light from magnetite crystals. Magnetite does not form until above 1060ºC and at 1222ºC hematite has not degraded, but at 1305ºC hematite has degraded to form magnetite in a limited oxygen atmosphere.

Figure 12.9 is a commercially prepared counter slab of quartzite from Brazil. It contains 1) a void area on a fracture which may have been randomly filled with scrap breccia, 2) hematite iron adjacent to the void and cracks where oxygen could have access, 3) Upper, the point that ties the original image to the enlarged detail. Hematite occurrence stops at this point and just a dark crack continues. At some point this bed of quartzite experienced an expanding event on this crack. This is the furthest point that opened up and oxygen had access. 3) Lower, this crack is at a different angle so it relates to a second point of shear. Both of these cracks had to already have occurred so when this third expansion event occurred, both previous cracks opened up to this point and white linears continue. This shows that while the oxygen availability stopped the temperature penetration on the linear continued. If air movement in the crack cannot continue, the elevated temperature that affected the iron had to have some other way to be transmitted in a linear. I suggest a linear moving out with a shock wave is one expression of localized heat that can pass through the matrix. This heating would be restricted to a circular lineament and not a general heating of the entire area. 4) An enlarged crystal of magnetite, identifying all of the smaller black grains as magnetite. The lack of these dark grains beyond 3, identifying the heating of the magnetite in the white strips has produced iron atoms. 5-7) Three different directions of planar fractures representing three different shear centers. Linear 6 may be an arc showing its center is closer.

The three fracture linears directions indicate three centers of shear. Representative from each set of linears show the results of heating and opening to oxygen all in one event. These three directions are sufficiently diverse in direction that a tectonic source of the shears seems highly improbable. It was not shoved from only one direction, and the timing does not suggest they happened millions of years apart. This quartzite slab has all of the characteristic of a PF, and suggest it records at least three impact centers and four impact events. While the exact origin location of the slab is not known, it gives an idea of the number of impacts that must be involved. This slab is not the result of a few individual impact scattered over a continent, but four impacts interacting in a single bed of quartzite.

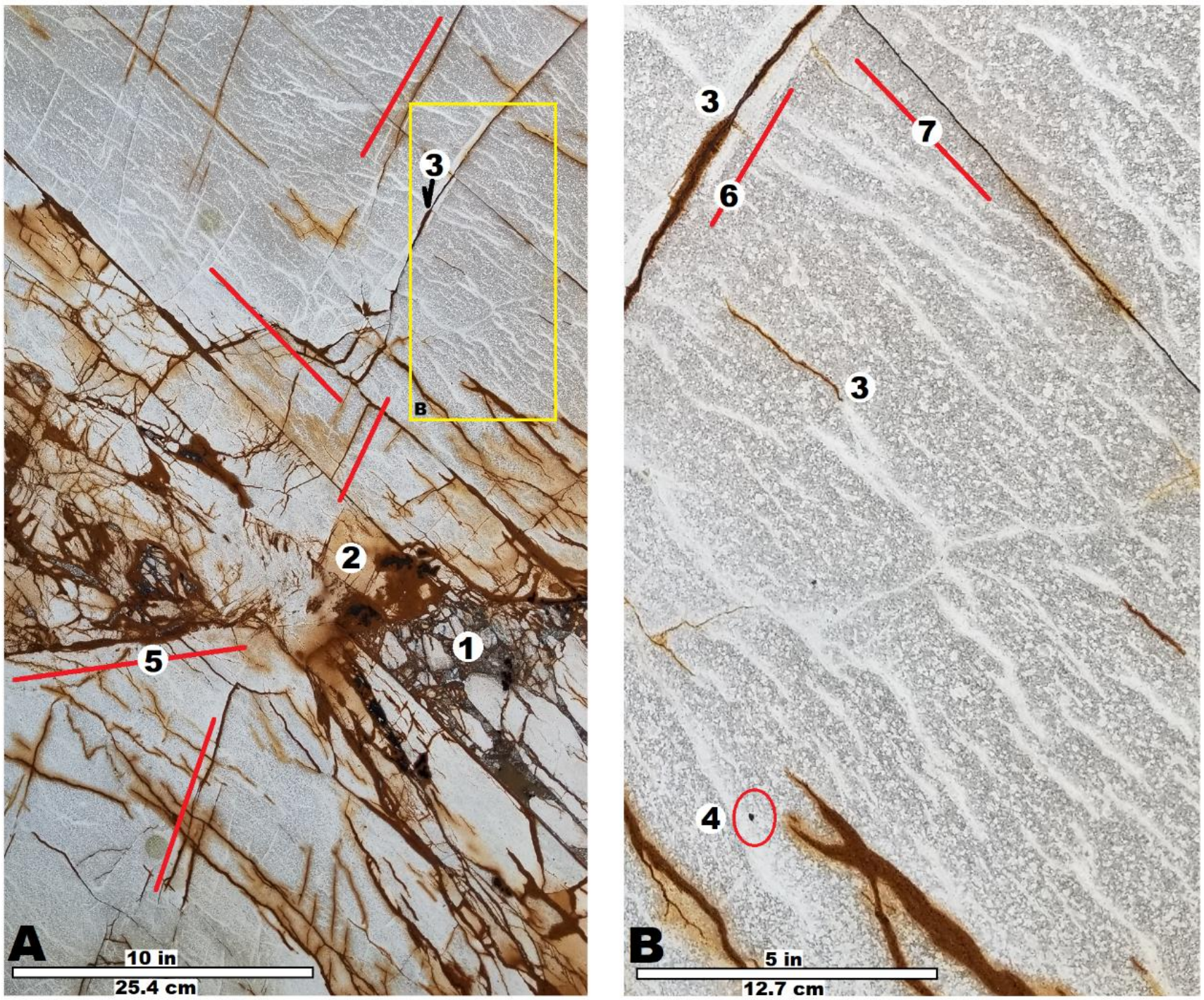

Figure 12.9: A) Slab of Quartzite. B) Detail from mid-upper right.

Seeing energy signatures

Chapters 3-5 addressed the Pacific Fracture Zones. At least nine of these linears (Table 3.2) are concentric to a center in the Kara Sea north of Siberia and are shown to have a common cross section, and all exhibit the same structure, which I am labeling the *energy signature of an impact*.

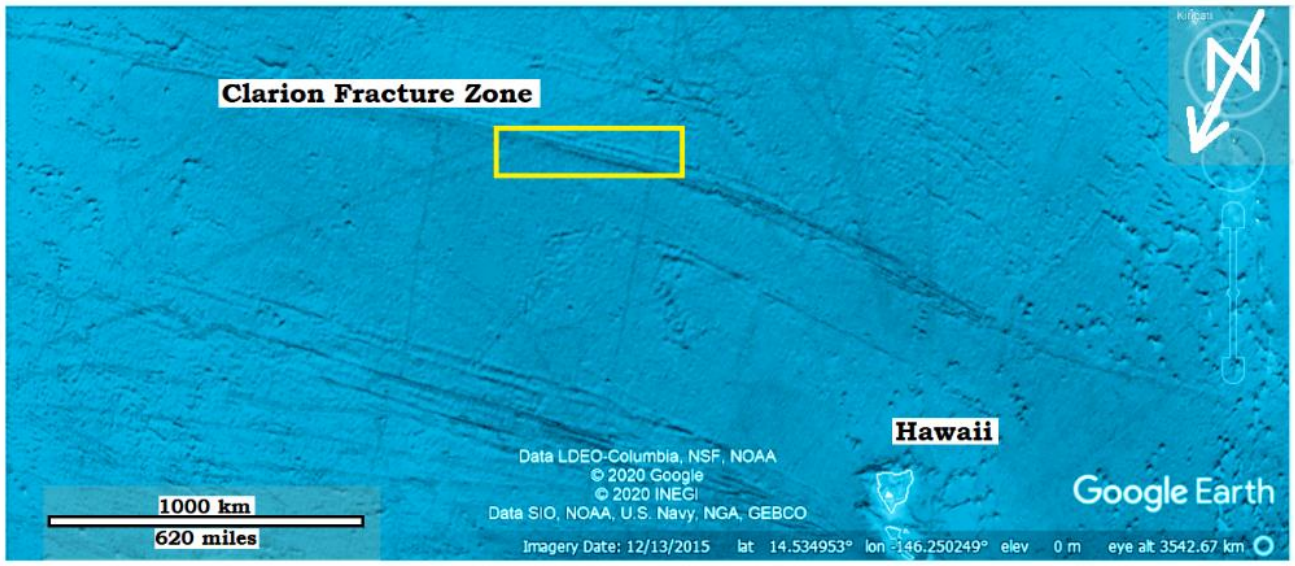

Figure 12.10: Clarion Fracture Zone showing location of detail in Figure 12.11 south of Hawaii Island. Note north is towards the bottom with shockwave traveling out of the bottom towards the south. Color enhanced to remove deep blue Google Earth adds to NOAA data.

The Clarion Fracture Zone (Figure 3.2) shares several structural features with the Altai Scarp (Figure 11.4), the Original Crater Ring (OCR) structure around Mare Nectaris on the moon. In Figure 12.11, we see “5 (AS)” and “8” are the upthrust expression of the shock wave, while “2” and “7” are the release wave valleys that follow the expanding shock wave. While the shock wave of the Clarion has almost a dual expression (compare Figure 12.11C to the cross section in Figure 3.4#2) the furthest ridge is smaller and less distinct, while the release valley shows similar variations [also similar to Krakatoa’s seismic waves, Figure 3.6]. This can be looked at as the energy peak and valley from the single impact has broken up into a short wave-train of energy by the time it has reached this point. This dual expression of shock wave ridge followed by the depressed release wave valley constitutes the energy signature of an impact.

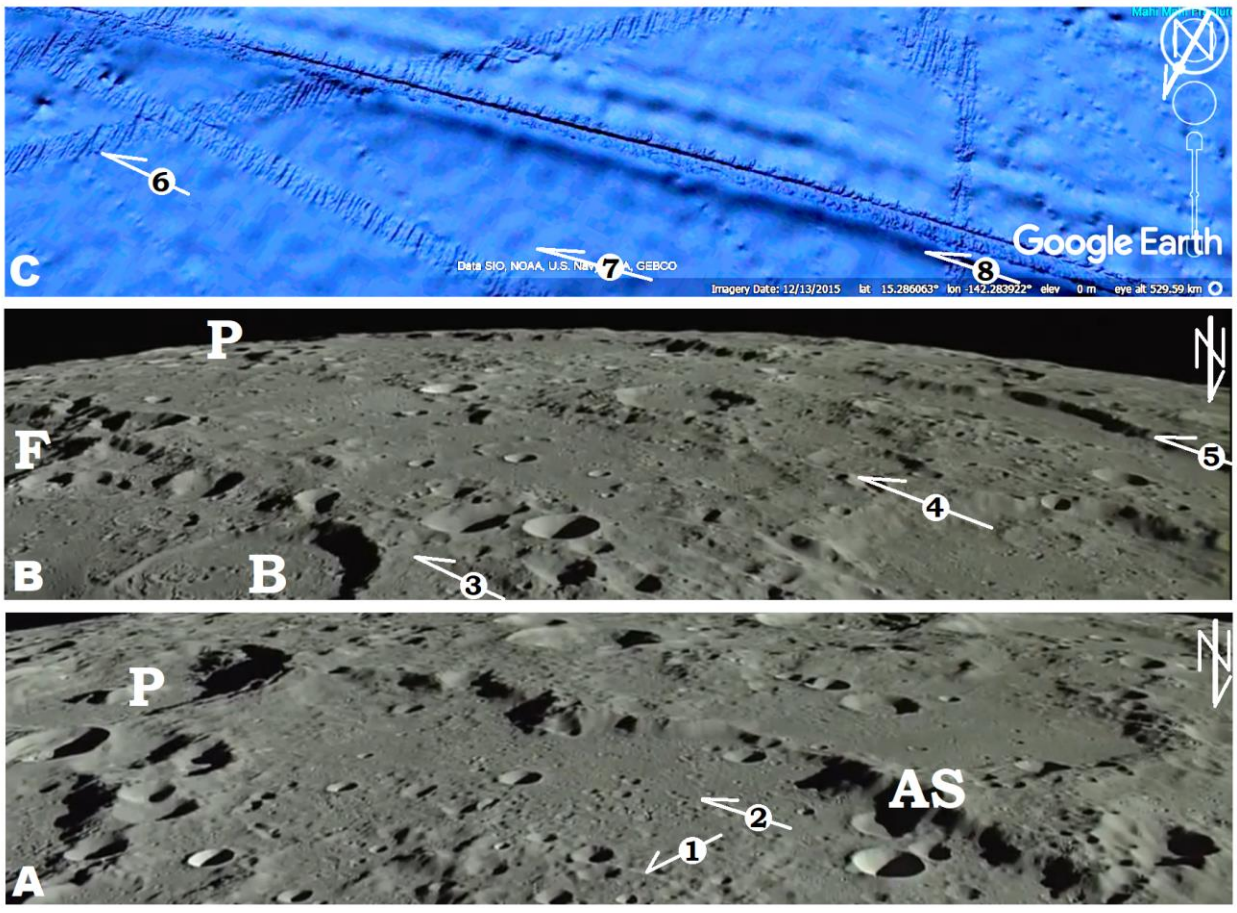

Figure 12.11: Comparing structure of the shock-release wave pair in Mare Nectaris (see Figure 11.4 for context) and Clarion Fracture Zone (see Figure 3.2 for larger context). A) Altai Scarp (AS) terminating in Piccolomini (P) crater on the left (west). (2) Identifies the release wave valley that occurs within the shock wave that extends from AS to the rebound wave’s slight ridge at (1). B) Shows the inner or open ring (3) just outside Fracastorius (F) and Beaumont (B) craters, and one (4) of several additional rings forming a small wave-train of mini-ridges across the plain. C) Google Earth image showing details of the Clarion Fracture Zone. “Tank-tracks” (6) are an anomaly of excess data in this line. The trailing edge of the release wave valley (7) and the sudden plunge from the shock wave peak to the release wave valley (8). (Image credit: A &B taken from JAKA/NHK 2009.)

Freundlich-Sharonov Basin

Figure 12.12 gives a broad view of the area surrounding Moscoviense and Freundlich-Sharonov basins on the farside of the moon. Looking at the yellow box detail, in Figure 12.13A shows a definite scarp heading north from the Spencer Jones crater, which is equivalent to the yellow linear between blue, low gravity, and red, high gravity, in the GRAIL gravity map. As this is an intermediate

gravity density, it corresponds to the sharp plunge from extremely high density to extremely low. A distinct release valley is not seen in the oblique view as many overlapping craters have obliterated it.

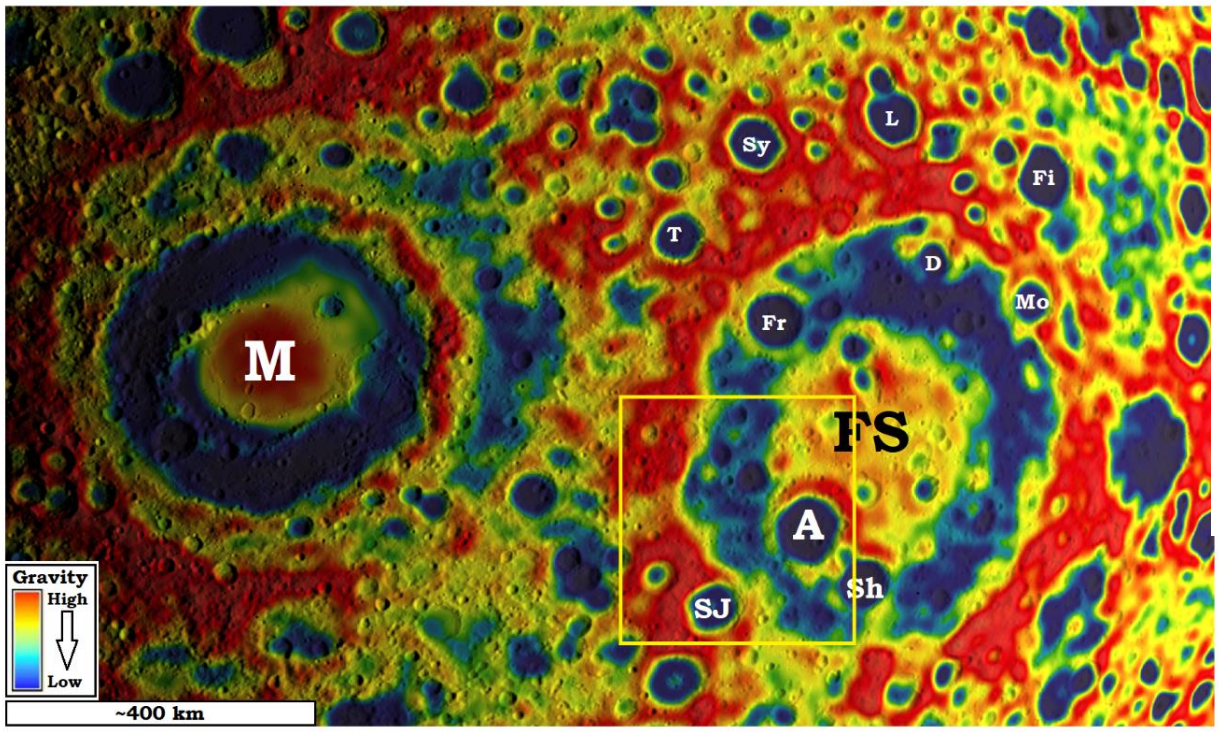

Figure 12.12: GRAIL image Moscoviense (M) and Freundlich-Sharonov (FS) Basins, with Anderson (A), Dante (D), Fitzgerald (Fi), Freundlich (Fr), Larmor (L), Morse (Mo), Sharonov (Sh), Spencer Jones (SJ), Shayn (Sy), and Trumpler (T) craters, on the farside of the moon. Yellow box is location of detail in Figure 12.13. (Image credit: NASA.)

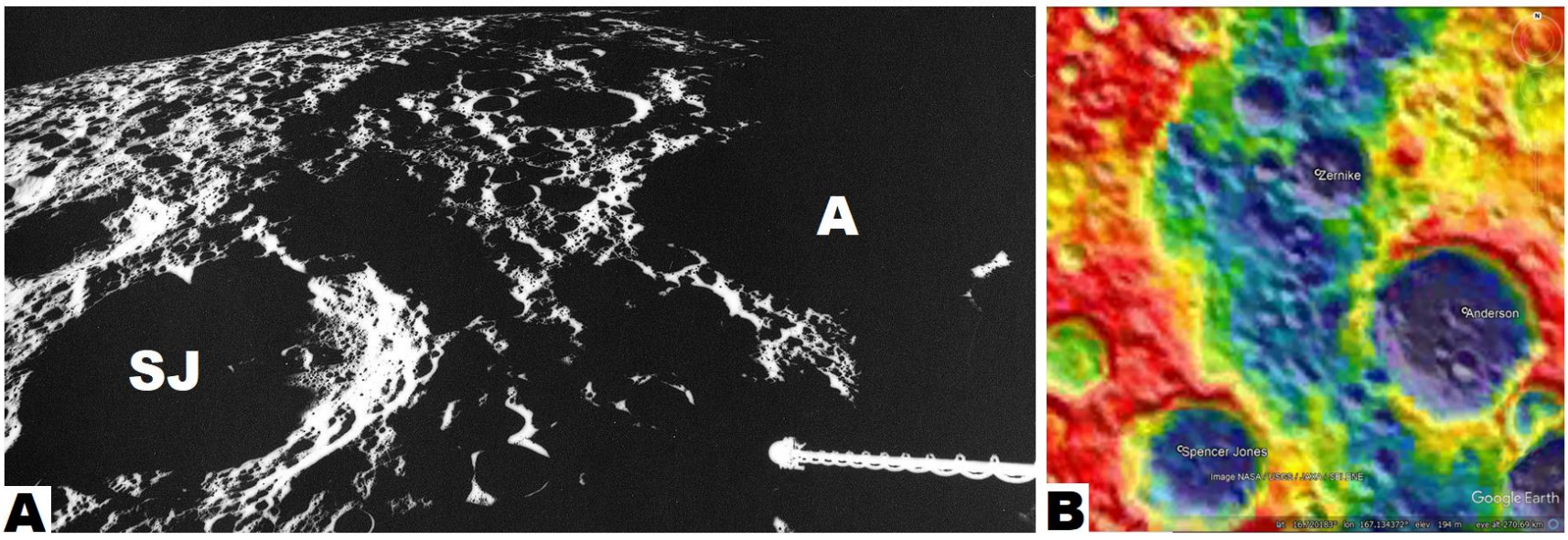

Figure 12.13: Oblique view of west edge between inner and OCR ring of Freundlich-Sharonov Basins between Spencer Jones (SJ) and Anderson (A) craters (Image credit: A) NASA, Apollo 16 image, 1972, credit: J. Stuby. B) NASA GRAIL fitted to Moon in Google Earth.)

Analyzing the Freundlich-Sharonov basin in Figure 12.12, the Sharonov, Anderson, Freundlich, Dante, and Morse craters show their low density surrounded by higher density of their OCR. Moving out to the Trumpler, Shayn, Larmor, and Fitzgerald craters show exactly the same and with another half-dozen or more craters and irregular area of low density make up a ring of low density outside the red ring of high density. Assuming impactor strikes at random locations and the occurrence of many lower gravity spots, yellow, within the red area, I propose the ring of prominent blue craters is an additional release wave valley where the blue centered craters maintained the otherwise dark blue area similar to the wide arc adjacent to the Moscoviense basin to the west.

In the manner of recognizing the bowl shaped depression of a crater in Crustal Thickness maps used in Chapters 10A and 11, Figure 12.14 recognizes the OCR for both the Moscoviense and Freundlich-Sharonov basins is in agreement with Figures 9.9, 10, and 13 and Figures 11.7-9. From the OCR a pattern of alternating rings can be seen in Red Relief map, Figure 12.15 for each basin separately and together.

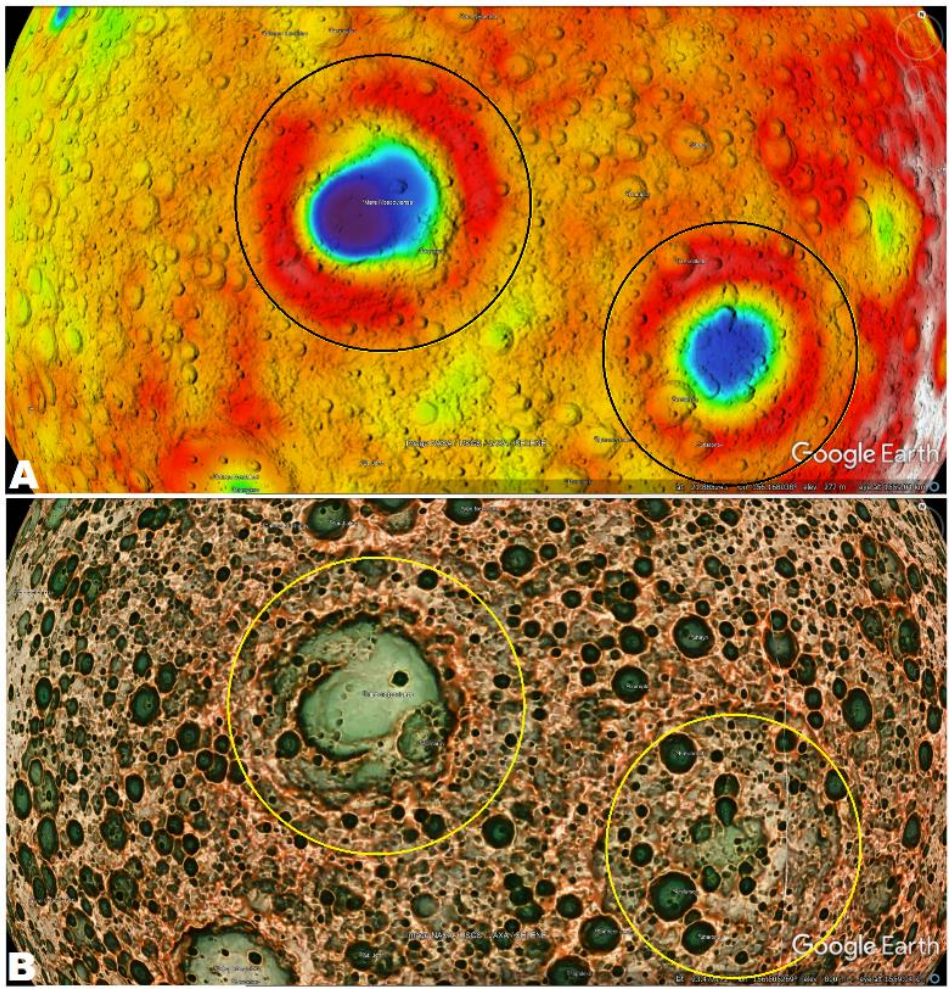

Figure 12.14: Recognizing the OCR from the bowl shape in A) Crustal Thickness map and transferring those circles to Red Relief map, (Image credit: A) NASA, Crustal Thickness overlaid on Google Earth Moon, B) Chiba 2017.)

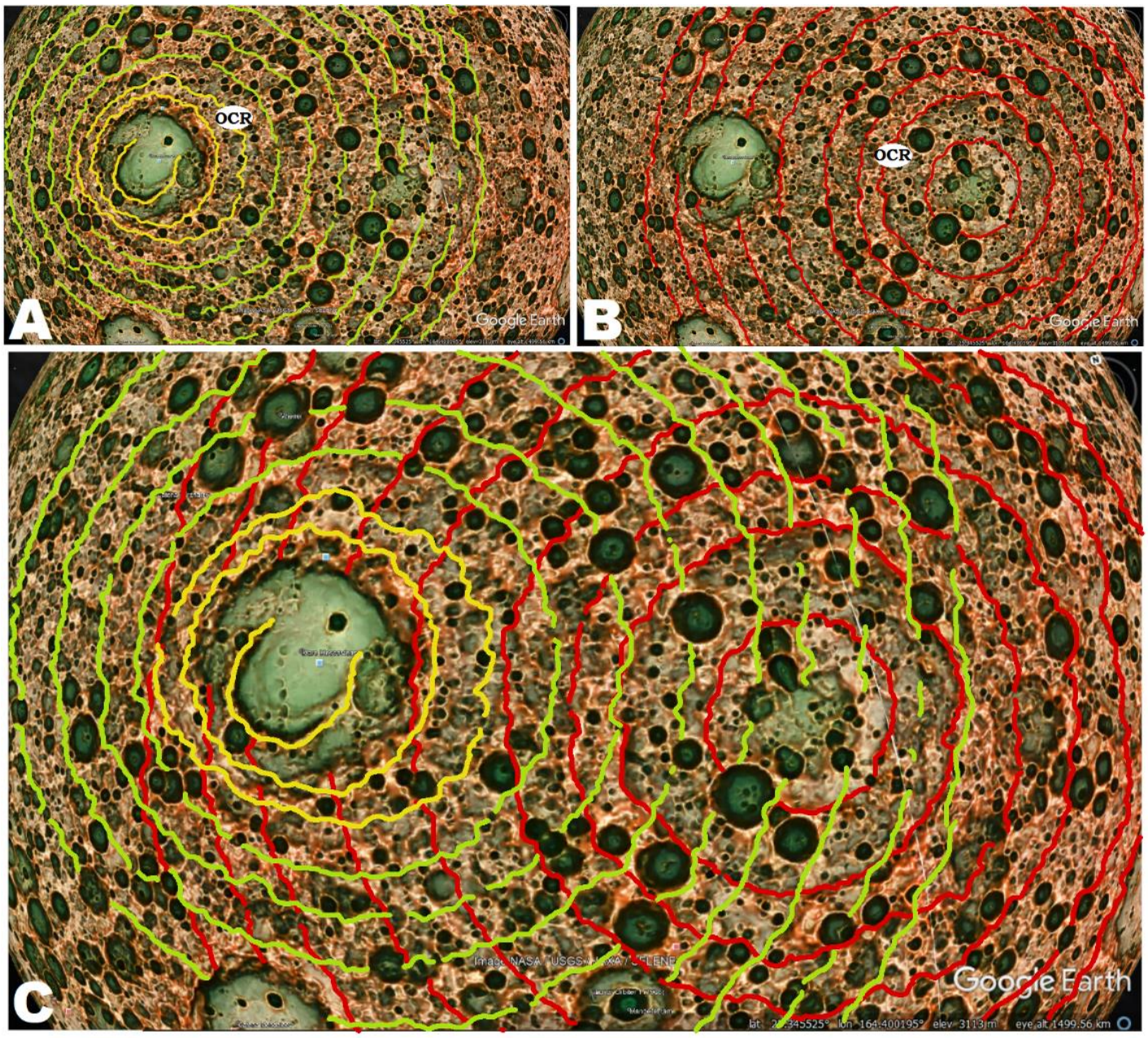

Figure 12.15: Red Relief overlay for Google Earth showing Moscoviense and Freundlich-Sharonov Basins with concentric rings as largely perfect circles distorted by smaller craters. (Image credit: Chiba 2017.)

Artemis Chasma

Located on Venus, Artemis Chasma is 75% of a nearly perfectly circular valley, ~2,100 km diameter, with the valley varying from 25-200 km width and 1-2 km depth (Bannister and Hansen 2010). Figure 12.16 shows at least six other craters that have had a distinct effect of displacing this release valley. The larger crater to the northwest shows it was instrumental in obliterating the missing 25% of the valley. The three cross sections of the valley show that smaller craters made a significant contributing to the final form of the cross section as seen around the Altai Scarp of the moon, Figure 8.10. But, as the release valley is expected to be inside the shock wave high (Figure 1.3), sections D and E, with their higher ridge on the inside of the valley shows the added energy of later impacts controls final topographic expression. The U-shaped valley bounded by two highs is consistent with the energy signature of a shock-release wave pair modified by additional later impacts.

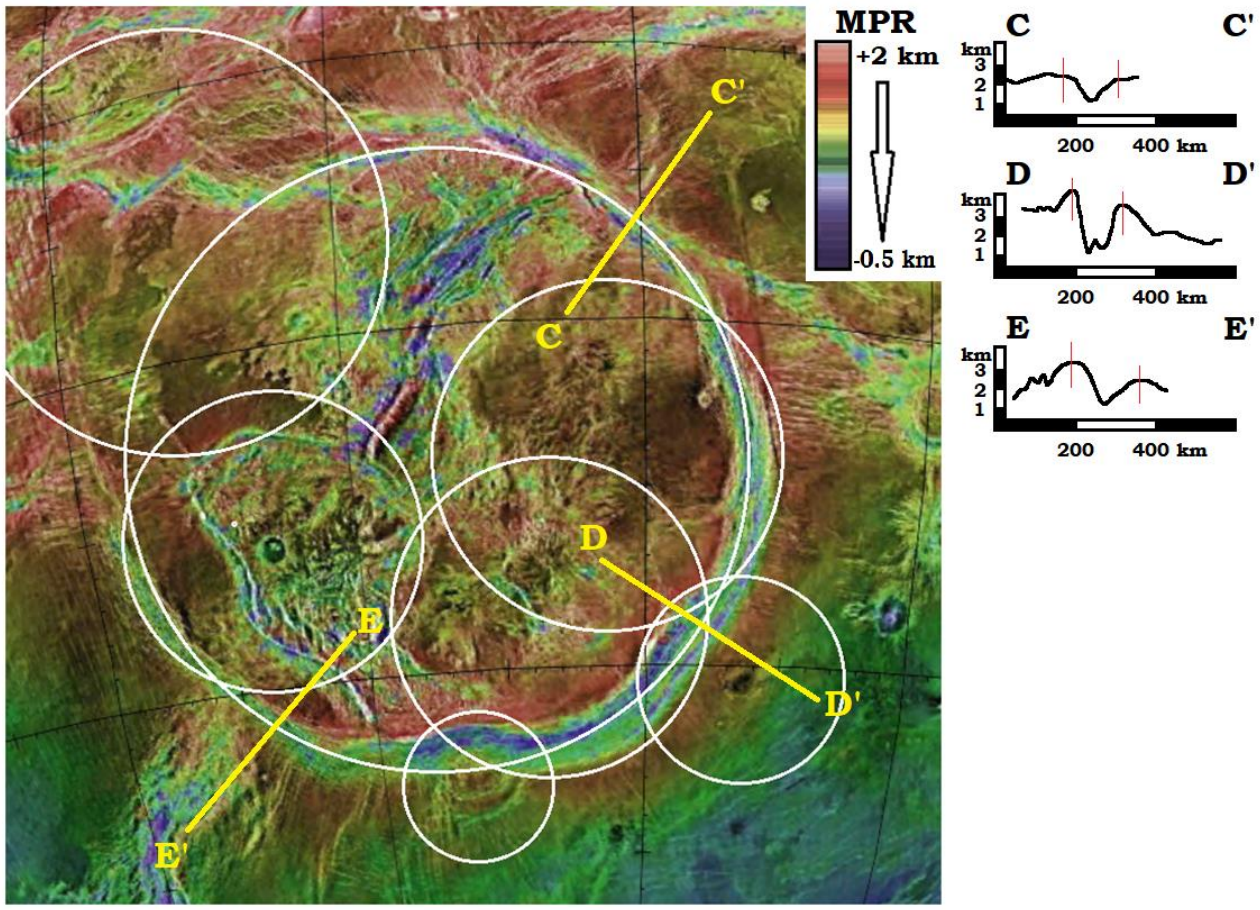

Figure 12.16: Artemis Chasma on Venus showing three cross sections through release valley, and six later craters that varied the location and recognition of that release valley. (Image credit: Hamilton 2001 overlaid on Google Earth by M. de'Hart.)

Seeing Lineament as Energy Signatures

The cratering process of impactors (Chapter 1) starts with the shock wave that first expresses itself through the crowning event in a bowl shaped depression I'll call the impact pit. This expression of the shock wave is immediately followed by the release wave (Figure 1.3). The sudden change from the shock wave to release wave is so abrupt, it is described as an "adiabatic approximation." This adiabatic point is defined as a point of such sudden change that heat and pressure do not have time to be conducted from particle to particle so is instead expressed as work. This work commonly is in the form of a density or topographic change or both changes to the rock.

Cratering Mechanics

Because cratering is an interaction between the shock and release waves, it cannot be formed by continued ballistic ejection as Shoemaker (1974) and Figure 8.3 suggest. Neither can it follow the basic pattern of Osinski and Pierazzo (2013) where they assume as the impacting body strikes Earth, it produces a shockwave by the vaporization of the impactor (As demonstrated by the skipped rock, Figure 12.2, where the puck escapes after the shock wave is produced.). All of the energy transfer is too rapid for any type of explosion after the initial contact and all energy transfer takes place within an adiabatic envelope.

This is shown in Figure 12.17. A) When the impactor strikes a contact pit is formed by the contact force. This may be the only force involved in forming the multitude of small conical pits presently on the moon's surface. But, larger impactors with greater force continue. B) The force of mass and supersonic speed generates a shock waves (red) and release wave (blue) exemplified by the immediate production of *melt* ejecta from the adiabatic conversion taking place between them (Lundberg 2016). C) As forces penetrate more rapidly, finely divided breccia may be produced from the substrate, but D) eventually an adiabatic "envelope" develops temporarily limiting the quantity of ejection until the approximate maximum size of the crater has been reached. This has taken milliseconds from time of impact. E) Once maximum size is reached the "envelope" burst laying back portions of the surface that were undermined, like in Meteor Crater (Figure 8.17). F) Evidence for the concept of an "envelope" is the force is driven down into the substrate further than the crater, opening up fresh radial fracture, or more likely, previous fractures from other impacts as seen in the Baldy and Verde CGRS which were opened up by ejecting breccia from the Meteor Crater (Figure 8.16 & 17). As these adiabatic faults then close they often capture part of the liquid breccia which they transported. This liquid breccia forms dykes that did not have to be

injected by a separate process. G) Contraction of the expanded craters follows with a push-up of a jetting event. This jetting event may only produce a small central peak as in Aristarchus crater (Figure 8.5), which still reflects the pattern of geology in the substrate below the crater floor, or brings up significant quantities of loose breccia (Figure 11.10) leaving a central ring.

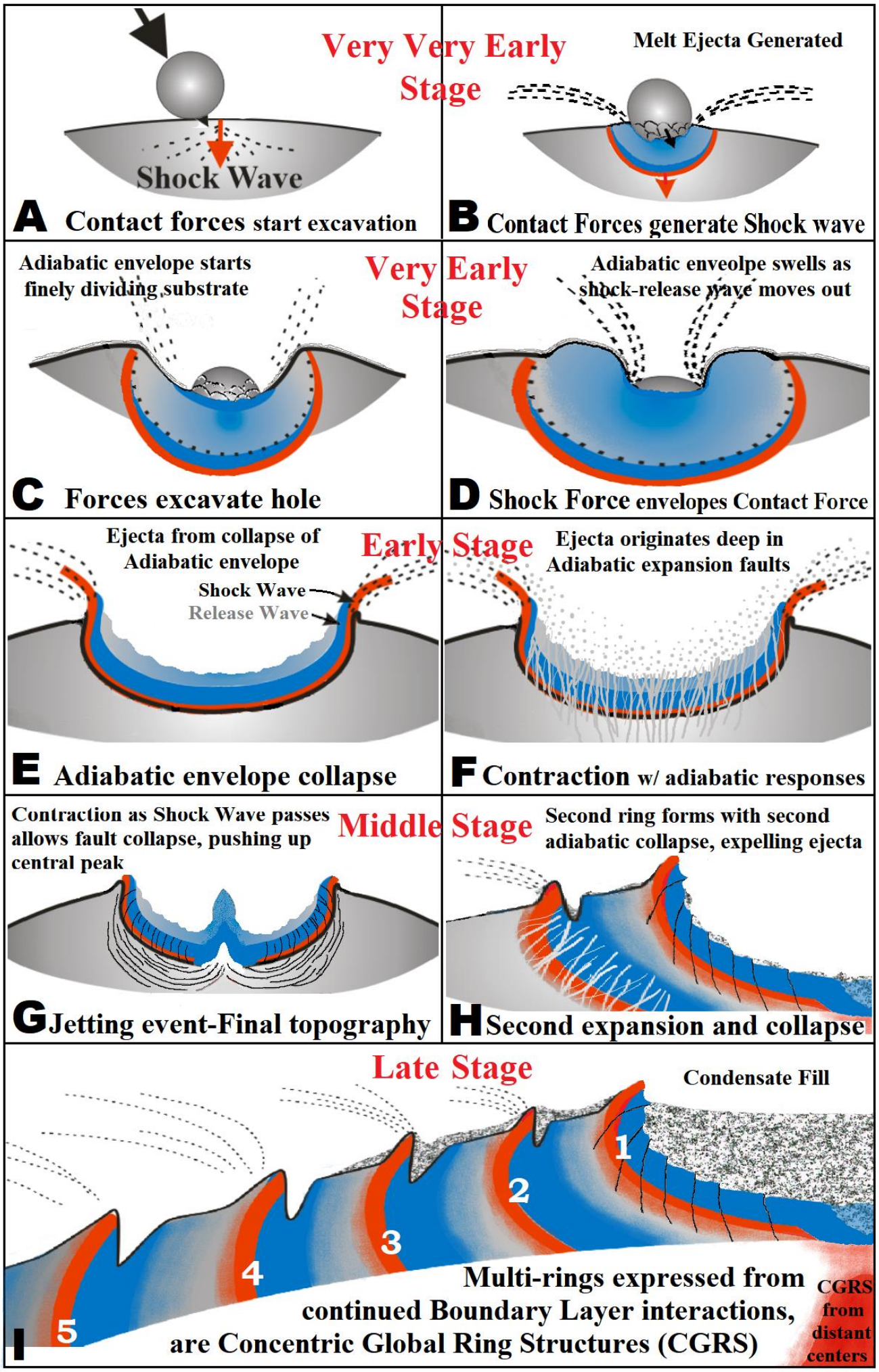

As the collapse of the jetting column breccia will result in the low gravity fill (dark blue) for the crater, it cannot be carrying compressed material from below the crater. Such collapse is essentially the last event within the original crater. H) The ever expanding shock-release wave moves outward to form a second adiabatic envelope with its expansion and opening of more adiabatic faults, the expulsion of ejecta and filling more dykes in the substrate. I) The processes are repeated again and again, with some rings more pronounced and some expressions breaking up into wave-trains of smaller rings as the energy signature of this impactor interacts with numerous other energy signatures from other impactors on the global surface occurring within the same area.

Figure 12.17: Sequence of cratering events following the energy signature concept.

Defined an energy signature as evidence of movement from extreme high to extreme low energy by way of an adiabatic dispersion where the excess energy contributed by the shock wave is converted to work as a means to get to the low energy of the release wave.

Demonstrating how this energy signature concept can be used to identify cratering events will be the thrust of the next chapter.

Acknowledgements

Much thanks to Maarten ‘t Hart who created the overlays for Google Earth Moon and Venus for me using cylindrical projection maps of the GRAIL with LOLA, LOLA, and Crustal Thickness map available from NASA at https://svs.gsfc.nasa.gov/4014, accessed April and May 2020, an d.

References

Africano, F., G. Van Rompaey, A. Bernard, and F. Le Guern. 2002. Deposition of trace elements from high temperature gases of Satsuma-Iwojima volcano. *Earth Planets Space* 54:275-286.

Bannister, R.A. and Hansen, V.L. 2010, Geologic map of the Artemis Chasma quadrangle (V-48), Venus: U.S. Geological Survey Scientific Investigations Map 3099.

Chiba, T. 2017. Topographic maps of the moon. Freely rotatable red relief maps of the moon globe. Asia Air Survey, Geospatial Information Authority of Japan. https://www.gsi.go.jp/chirijoho/chirijoho41026.html, accessed 12/20/2019.

Clanet, C., F. Hersen, and L. Bocquet. 2004. Secrets of successful stone-skipping. *Nature* 427(6969:29.

French, B.M. 1998. *Traces of Catastrophy: A Handbook of Shock-Metamorphic Effects in Terrestrial Meteorite Impact Structures.* LPI Contribution 954. Lunar and Planetary Institute, Houston, TX. 120p.

Giere, R., W. Wimmenauer, H. Müller-Sigmund, R. Wirth, G.R. Lumpkin, and K.L. Smith. 2015. Lightning-induced shock lamellae in Quartz. *American Mineralogist* 100(7):1645-1648.

Hamilton, C. 2001. Venus, equal-area projection, NASA, Magellan Mission.

Hryanina, L.P., 1999. The bouquet of the meteorite craters in the epicenter of Tunguska Impact 1908 year. *Lunar and Planetary Science XXX*, Houston, Lunar Planetary Institute.

ION Geophysical. *YucatanSPAN* https://www.iongeo.com/wp-content/uploads/2019/03/DS_GEO_YucatanSPAN.pdf. Accessed 11/14/2019.

JAKA/NHK. 2009. KAGUYA taking “Rupes Altai” by HDTV. https://www.youtube.com/watch?v=dJA-U6ICXeY&index=203&list=PLDA9C6AA8E11F7E56, accessed 4/1/2020.

Kvasnytsya, V., R. Wirth, L. Dobrzhinetskaya, J. Matzel, B. Jacobsen, I. Hutcheon, R. Tappero, and M. Kovalyukh. 2013, New evidence of meteorite origin of the Tunguska cosmic body. *Planetary, Space Science* 84:131–140.

Lundberg, L.B. 2016. Impact Geology: the basics. http://www.impact-structures.com/wp-content/uploads/2017/09/Impact-Final-2.pdf, accessed December 2, 2019.

Osinski, G.R. and E. Pierazzo. 2013. Impact cratering: process and products. In: *Impact Cratering: Process and Products, First Edition*, Osinski, G.R. and E. Pierazzo, (editors) Blackwell. Publishing Ltd., West Sussex, UK.316 pps.

Shoemaker, E.M. 1974. Barringer Meteorite Crater, Coconino County, Arizona. In *Guidebook to the Geology of Barringer Meteorite Crater, Arizona*. Shoemaker, E.M. and S.W. Kieffer (editors) Publication no. 17, Reprinted 1988, Center for Meteorite Studies, Arizona State University, Tempe, Arizona: 1-11.

Strachey, R. 1888. ‘On the air waves and sounds caused by the eruption of Krakatoa in August, 1883”. In G.J. Symons (editor), *Report of the Krakatoa Committee of the Royal Society*. Harrison and Sons, London, 494 pages.

Vannucchi, P., J.P. Morgan, D.D. Lunga, C. Andronicos, and W.J. Morgan. 2015. Direct evidence of ancient shock metamorphism in the site of the 1908 Tunguska event, *Earth and Planetary Science Letters* 409:168-174.

Watchorn, B. 2013. Meteorite impact structures and their relation to mineralization in the eastern Yilgarn. https://www.youtube.com/watch?v=l0HdKnHomeA, accessed 6/22/2020.

Wharton, J.L. 1888. “On the seismic sea waves caused by the eruption of Krakatoa, August 26th and 27th, 1883”. In G.J. Symons (editor), *Report of the Krakatoa Committee of the Royal* Society. Harrison and Sons, London, 494 pages.